

RESEARCH ARTICLE

Laser Texturing of Soda Lime Glass Surface for Hydrophobic Surface in Wenzel State

K.A. Nur Najwa¹, Z. Najihah¹, S.N. Aqida^{1,2,*}, I. Ismail^{2,3} and M.S. Salwani¹

¹Faculty of Mechanical and Automotive Engineering Technology, Universiti Malaysia Pahang Al-Sultan Abdullah, 26600 Pahang, Malaysia

²Automotive Engineering Centre, Universiti Malaysia Pahang Al-Sultan Abdullah, 26600 Pahang, Malaysia

³Faculty of Manufacturing and Mechatronics Engineering Technology, Universiti Malaysia Pahang Al-Sultan Abdullah, 26600 Pahang, Malaysia

ABSTRACT - Glass surfaces tend to be hydrophilic when exposed to water resulting in a low water contact angle and high adhesion. Fabrication on a glass surface with low water adhesion can minimize the droplet's adhesion conduct self-cleaning, and improve the cleanliness of the glass surface. This paper presents surface texturing of the soda-lime glass surface by laser processing three different patterns to improve water contact angle with low water adhesion on the modified glass surface. A design experiment method was developed to determine the effects of laser parameters on the glass surfaces. The laser parameters used are laser power between 0.45 and 1.05W and scanning speeds of 210, 420, and 600 mm/min. The effects of laser parameters on surface morphology, water contact angle measurement, and average surface roughness, R_a were investigated. The characterization was conducted for surface morphology, two-dimensional surface roughness profile, and water contact angle. The results show that the highest water contact angle obtained after laser texturing is up to 125.29° compared to the as-received surface with a contact angle of 32.35° . The highest water contact angle resulted from 420 mm/min scanning speed and 0.45 W of laser power, responding to the surface with a minimum range of R_{ax} and R_{ay} of 0.96 and $1.5 \mu\text{m}$. These findings are significant for designing surface modification of self-cleaning glass surface applications like the automotive windscreens, and window panels for high-rise buildings.

ARTICLE HISTORY

Received : 12th May 2023

Revised : 16th Nov. 2023

Accepted : 14th Dec. 2023

Published : 20th Mar. 2024

KEYWORDS

Laser texturing

Hydrophobic

Soda-lime glass

Water contact angle

Wenzel state

1.0 INTRODUCTION

Hydrophobic and superhydrophobic properties achieved on various material surfaces such as metals, glass, ceramics, polymers, and composites can be fabricated with various methods, either chemically treated or modified physically [1] - [3]. Application of modified hydrophobic surfaces is being applied for various industries and research-based scenarios that require hydrophobic surfaces for better quality and results. Incredible improvement and functional performance of hydrophobic surfaces led to more discovery and research [4]. Applications of glass surfaces like solar cells, car windshields, mirrors, and window glasses for outdoor applications experienced water contact and exposure to sunlight [5]. The surface is easily contaminated with dust particles along the glass surface during the rainy season [6]. Hydrophobic properties have a self-cleaning effect when water contact is rolled off instead of pinned to the surface. The roll-off water droplets collect dust particles attached to the surface thus improving the cleanliness of the glass surface [7]. Besides glass surfaces, this property can be applied on various surfaces that require self-cleaning properties. This application can reduce the cost of cleaning while maintaining less fouling on the surface [8].

Surface modification is a useful method to improve materials such as adhesion properties, hydrophobicity, hydrophilicity, roughness, surface tension, and surface energy [9], [10]. Surface morphology is one of the important properties of a material, along with the composition and structure of the material surface [11]. Surface composition and structure are usually different from the bulk composition, where the surface atoms are surrounded by other atoms in all directions, and then bonded to other atoms from one side, which results in surface energy [12]. Surface texturing is widely used to provide beneficial functions by modifying the outermost layer [13]. Surface textured material can alter the surface wettability by inducing roughness to attain hydrophobic, superhydrophobic, and omniphobic surfaces [14]. A superhydrophobic surface can repel water at a larger contact angle of $>150^\circ$ [15] - [18]. Functional needs for automotive, aerospace, marine, medical, nuclear reactor, textile, clinical diagnostic, and sensing applications drive the majority of hydrophobic and superhydrophobic surfaces and coatings [19]. In nature, the lotus leaf is an icon of superhydrophobicity with self-cleaning properties, as it is covered with wax and an abundance of micro-sized papillae that lead to surface roughness [20]. The superhydrophobic metal surface has self-cleaning characteristics to prevent dust, rain, and fog adhesion and excellent anti-fouling properties in textile industries. Because the adhesive forces between water and glass are strong enough to pull water molecules out of their spherical configuration, water on clean glass tends to spread and form a thin film over the glass surface. Thus, glass becomes hydrophilic toward water [21], [22]. A combination of femtosecond laser irradiation and chemical treatment with a salinization solution has been shown in previous studies on the hydrophobicity of soda-lime-silica glass surfaces to be able to change the surface from hydrophilic to superhydrophilic and to hydrophobic, with contact angles ranging from below 20° to approaching 125° [23].

Changes in surface roughness have been studied, and several methods have been used. When glass is textured at the microscale, it creates a rough surface with features such as pillars, bumps, or ridges. These microfeatures alter the surface topography, increasing the surface area and reducing the solid-liquid contact, thereby enhancing the hydrophobic behavior. The presence of microfeatures on the glass surface can lead to the following effects such as surface roughness. Researchers discovered that after texturing, the grooves' roughness varies depending on the laser settings. In turn, this roughness affects wettability [23]. There are two processes used to generate hydrophobic surfaces, which are single-step processes and multi-step processes [24]. Single-step processes create surface roughness and deposition of low surface energy material in one step, while the multi-step processes have at least two steps which include surface roughening by different fabrication methods and follow-up by modification of the roughened surface using low surface energy coatings. The behavior of water droplets on a surface is affected by surface energies and wettability. A higher energy state of the surface usually exhibits hydrophilic properties with a smaller contact angle, while lower surface energy results in a hydrophobic surface with a higher contact angle [20]. Additionally, hydrophobic properties can be used as a preventative step to reduce corrosion due to water. An experiment by Liu et al shows a reduction in the corrosion rate of the copper surface by constructing microscale structures with superhydrophobic properties on the surface [25].

Various laser types have been reported in the laser texturing of glass surfaces for hydrophobic properties. Lin et al. used a femtosecond laser with a wavelength of 1030 nm and a maximum average power of 40 W [26]. The parameter of laser pulse varied from 20 μJ to 100 μJ , single pulse per point, and repeated 2 – 5 times with identical gradient on silica glass surface with 99.99% purity. Multiple ultrafast laser pulse ablation processes produced micro-pit array with self-organized nanostructures. Bing et al. used an amplified Nd:YVO₄ laser system with a wavelength of 1064 nm, output power of 14 W, average pulse energy of 35 μJ , and spot size of 20 μm to produce periodic microgrooves [27]. Silica glass, soda-lime glass, and solar glass have been reported for hydrophobic surface study. The contact angle of the as-received glass surface is 57° which indicates hydrophilicity [28]. Using the laser irradiation process, the glass surface can be modified into superhydrophilic or superhydrophobic. In this study, the soda lime glass surface was textured using a 450 nm wavelength laser for enhanced contact angle. The effects of laser parameters on textured soda-lime glass surface roughness, morphology, and water contact angle (WCA) were investigated.

2.0 METHODOLOGY

The material used in this study is soda-lime glass, with a thickness of 1.0 mm and a dimension of 76×26 mm, with the chemical composition given in Table 1. Sample processing was designed at four parameters, line distance, patterns, scanning speed, and laser power. Patterns were selected as categorical factors compared to others that were set as numerical; 3 levels were selected for numerical factor, line distance (in mm), laser power (in Watts), and scanning speed (in unit mm/min), while the responses are WCA (in degree), and average surface roughness, Ra (in μm). The glass surface was textured with three different patterns as shown in Figure 1 where the perpendicular line distance between the patterns differed as, in pattern 1 the line distance varies between 0 and 1.0 mm, whereas in patterns 2 and 3, the line distance is fixed at 0.5 mm and 1.0 mm respectively.

Table 1. Chemical composition of glass

Oxides	SiO ₂	Na ₂ O	K ₂ O	CaO	MgO	Al ₂ O ₃	Fe ₂ O ₃	SO ₃
wt.%	72.20	14.30	1.20	6.40	4.30	1.20	0.03	0.30

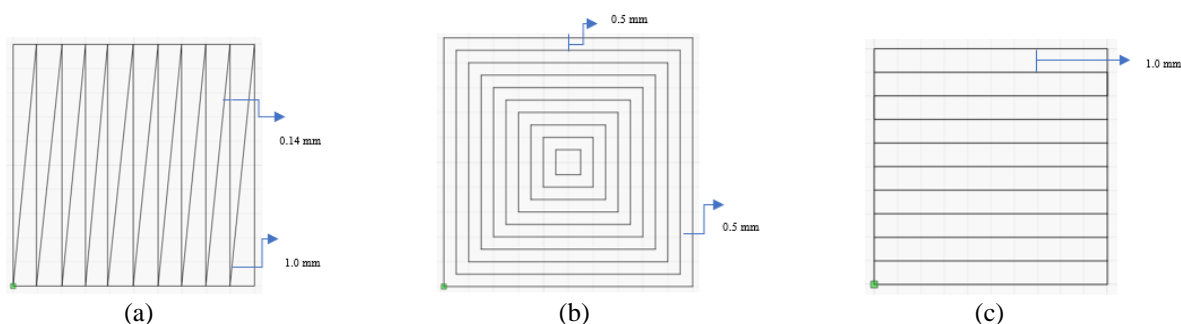


Figure 1. Laser textured soda-lime glass surface for (a) pattern 1, (b) pattern 2, and (c) pattern 3

Surface texturing of glass surface was conducted using a blue diode laser machine with continuous wave processing mode, a laser wavelength of 450 nm, a maximum output power of 15 W, a laser spot area of 0.08 mm × 0.1 mm, and a focal length of approximately 18 mm. The laser texturing setup is shown in Figure 2. A precise sample thickness is required to ensure that the laser spot is focusing on the glass surface. Unprocessed soda-lime glass will undergo a standard clearing process [28] with ethanol and deionized water cleaning before furthering up for laser processing with the range of parameters tabulated in Table 2 using the direct method of texturing as in Figure 2.

The WCA of the textured glass surface is measured using the sessile drop technique setup. The reagent used in this experiment was Type II reagent water (distilled) by ASTM D1193. The measured contact angles of water on the samples

were conducted according to the Practice of ASTM D7334 using a Hamilton microliter syringe [29]. A water droplet volume of 3.3 μl was deposited on the laser-textured glass surface and was measured rapidly (within 30 s of depositing the drop) to avoid changes in angle as the water evaporated [30]. The water droplet images were captured and converted to grayscale mode and then transferred to ImageJ software. Further analysis of water contact angle in ImageJ software was carried out using the Low Bond Axisymmetric Drop Shape Analysis (LB-ADSA) plugin. The interface of Drop Analysis software is shown in Figure 3(b).

Table 2. Design of experiment for laser texturing of glass surface

Standard Order	Speed (mm/min)	Power (W)
1	210	0.45
2	210	0.75
3	210	1.05
4	420	0.45
5	420	0.75
6	420	1.05
7	600	0.45
8	600	0.75
9	600	0.75

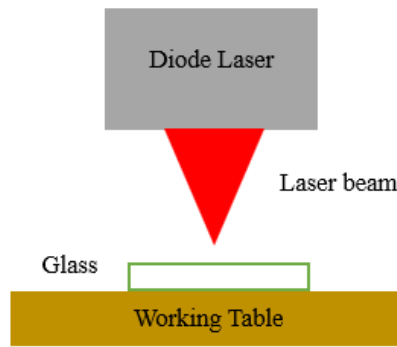


Figure 2. Schematic diagram of laser texturing of glass set-up

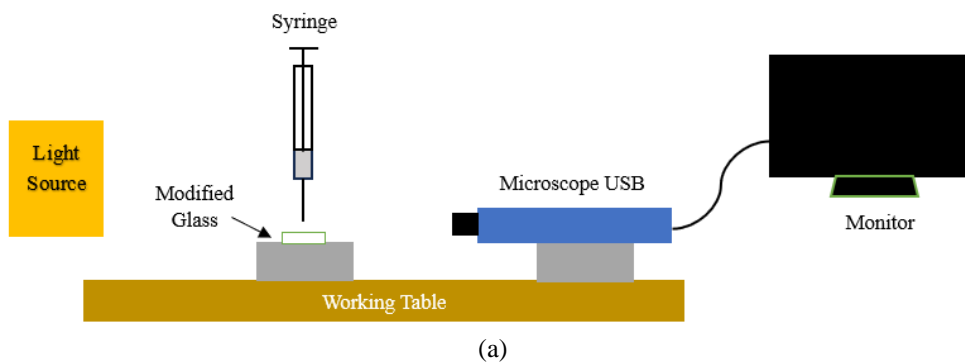
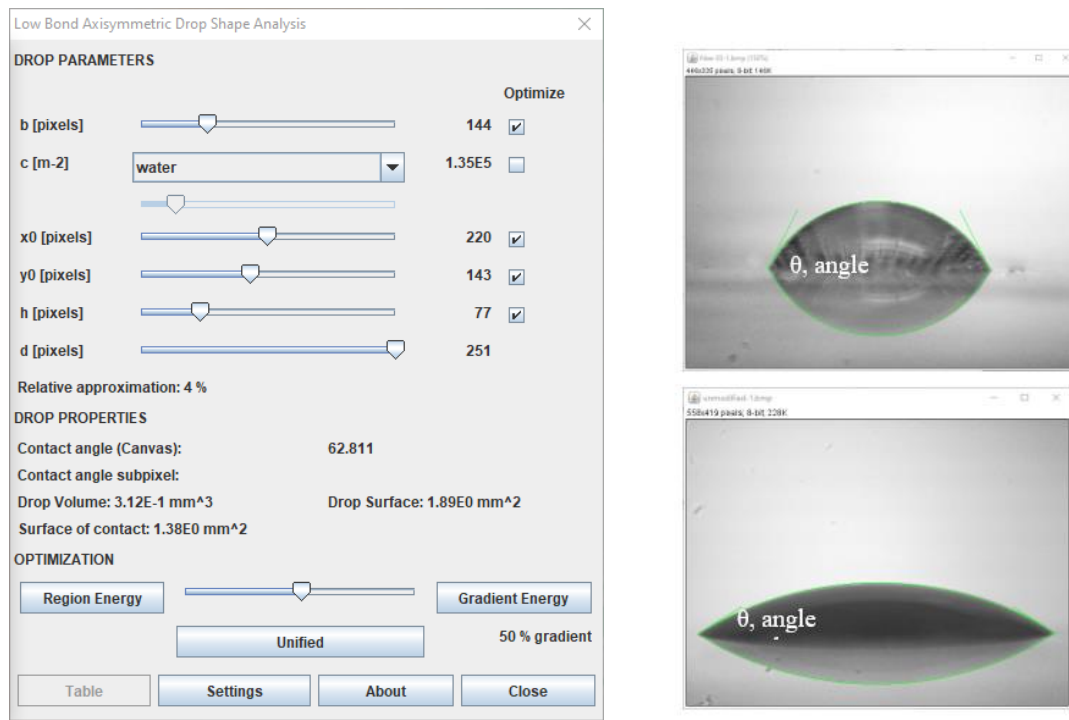


Figure 3. (a) Schematic setup of sessile drop test



(b)

Figure 3. (cont.) (b) The interface of Drop Shape Analysis for calculating water contact angle

The surface morphology and average surface roughness of textured glass were measured using a laser confocal microscope according to the international standard ISO 25178. The Olympus laser confocal microscope from the LEXT line-OLS 5000 by Japanese Olympus was used to investigate the effects of laser parameters on crack formation for different patterns and line distances. The surface profile was taken at three different sections along the x-axis which is parallel with the laser direction and in the y-axis, which is perpendicular to the laser process direction, as shown in Figure 4. The grooves on the glass were measured using the Olympus BX53 upright microscope, it is an upright metallurgical microscope with superior image clarity at 5 \times , 10 \times , 20 \times , 50 \times and 100 \times magnifications and for the glass sample, a 20 \times magnification was used.

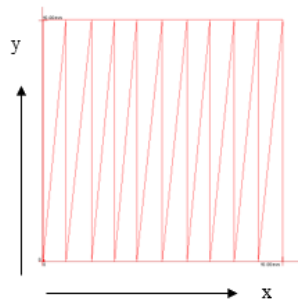


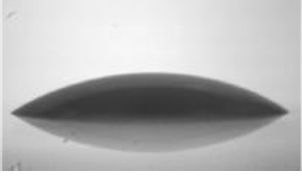
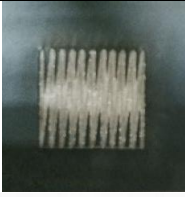
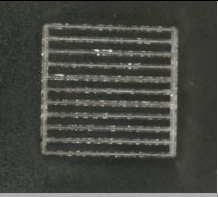
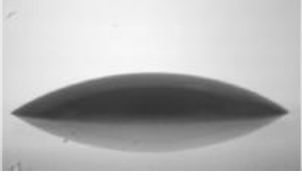
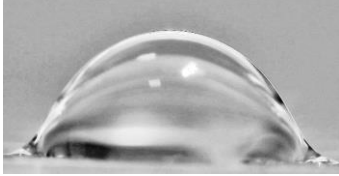
Figure 4. Surface profile measurement (x) parallel and (y) perpendicular to the laser direction

3.0 RESULTS AND DISCUSSION

3.1 Water Contact Angle

Laser-textured glass surface exhibits different WCA at different laser power and scanning speed. The resulting contact angles can be seen in Table 3 where the flat unmodified glass surface has hydrophilic properties with a 32.35 $^\circ$ WCA. After texturing, the contact angle for each pattern increased up to 125.29 $^\circ$, 116.12 $^\circ$, and 101.18 $^\circ$, respectively. Overall, the WCA increases after laser surface texturing, where the hydrophilicity of the glass surface is reduced, approaching hydrophobic. Apart from laser parameters, the WCA was affected by the line distance between the patterns. The highest WCA is in pattern 1 where the line distance varies between 0 and 1 mm. Whereas, in pattern 2, the WCA is lower as the line distance is fixed at 0.5 mm. The lowest contact angle is in pattern 3 with a line distance of 1 mm.

Table 3. Water contact angle of (a) unmodified glass surface, (b) laser textured glass at 0.45 W, (c) laser textured glass at 1.05 W, and (d) laser textured glass at 1.05 W

(a) Unmodified Glass	(b) Pattern 1	(c) Pattern 2	(d) Pattern 3
			
			
32.35°	125.29°	116.12°	101.18°

A relationship between WCA and laser power to scanning speed ratio is shown in Figure 5; the graph shows the value of the ratio at the highest WCA for each pattern, for pattern 1 the highest WCA was at 1.07 ratio and the R^2 was at 0.9947 and for pattern 2 the highest WCA was at 1.75 ratios and recorded the 0.3677 R^2 value and at ratio 5.0 for pattern 3 had the lowest value R^2 with 0.0428. R^2 value. R^2 also known as the coefficient of determination is a measure for measuring linear regression models, it also indicates the percentage and measures the strength of ratio and WCA collectively on a convenient 0 – 100% scale. As shown in Figure 5, pattern 1 explains 99% of the relationship while pattern 2 is 37%, and pattern 3 with 0% represents the relationship but does not explain any of the variation of WCA and laser power to scanning speed ratio.

The trend for patterns 1 and 2 is slightly similar because it recorded the lower ratio and indicated the highest WCA and pattern 3 observed the higher ratio of the relationship with the highest WCA. Varying laser power and scanning speed significantly alter the water contact angle measurement, however, lower laser power may offer a greater water contact angle. In Song et al. surfaces treated by the low-energy laser become more hydrophobic while at high energy laser, resulting in more hydrophilic properties. It is proven by Song et al that the surfaces treated by the low-energy laser become more hydrophobic while high energy laser results in more hydrophilic properties. The study shows that the energy affected by the laser power and surface structure affected by the scanning speed, and the parameter of laser power had a larger impact on the wettability compared to the scanning speed [31]. As laser power increases, the water contact angle decreases compared to the as-received material as the work of adhesion energy increases when laser power density increases [32].

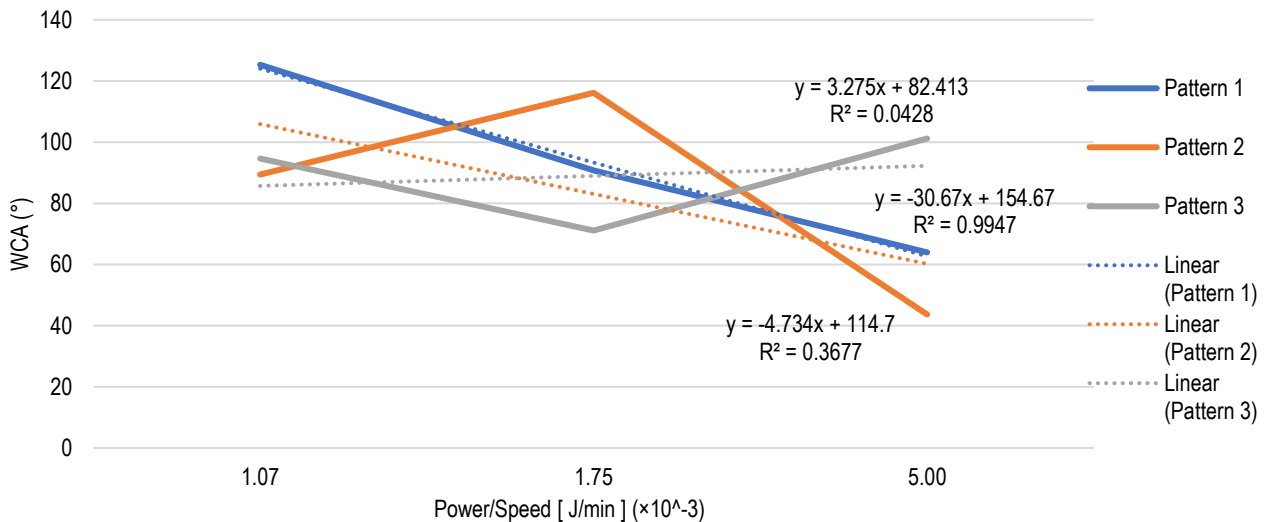
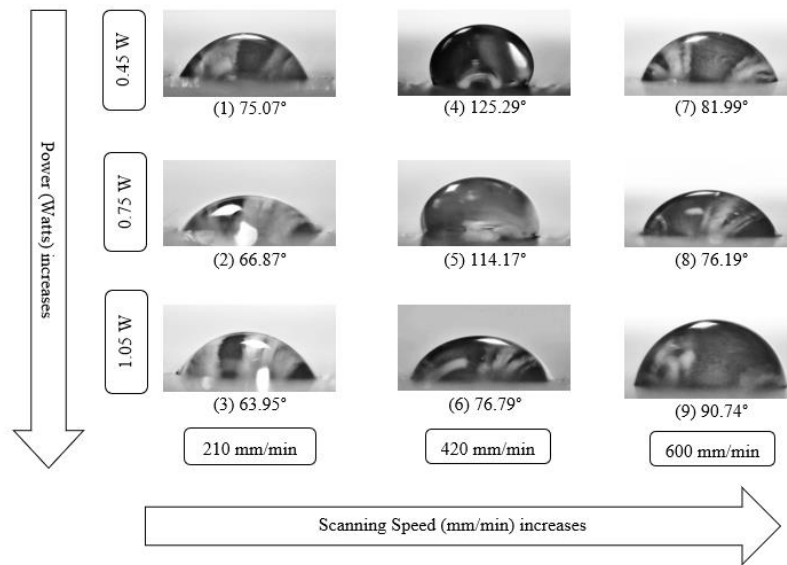
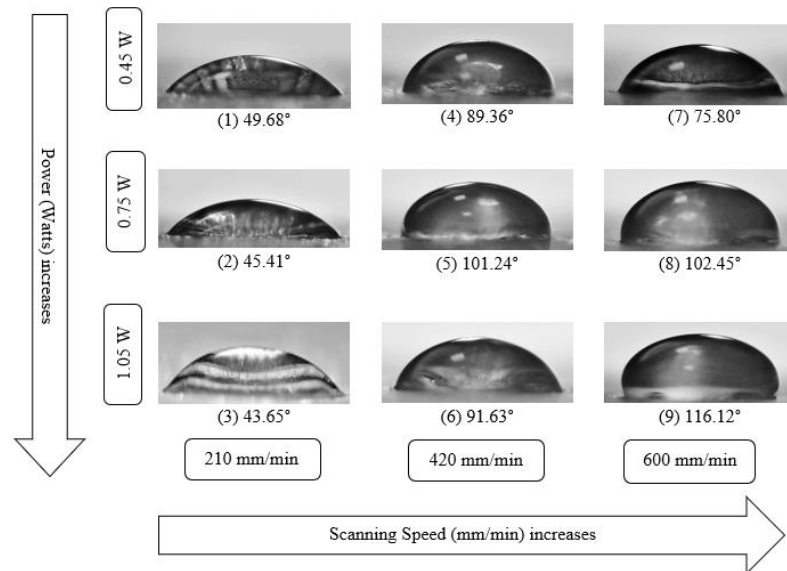


Figure 5. Water contact angle trend as a function of laser power to scanning speed ratio

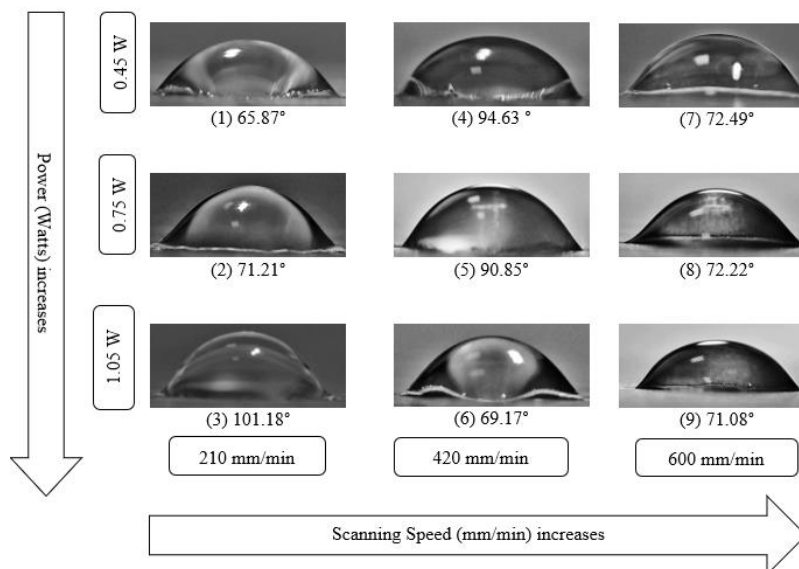
Referring to pattern 1 in Figure 6(a), the WCA ranges from 63.95° to 125.29°. At 210 mm/min and 420 mm/min scanning speed, the decreasing trend of WCA is observed as the laser power increases, while at 600 mm/min scanning speed the WCA ranges between 76.19° (in sample 8) and 90.74° (in sample 9). A similar result was reported by Jing et al. Factors like surface roughness, line distance, and pattern affect the wettability of laser-modified glass [33]. Sample 4 records the highest WCA of 125.29° at a laser power of 0.45 W and scanning speed of 420 mm/s. Sample 3 recorded the lowest WCA of 63.95° at 1.05 W and 210 mm/s laser power and scanning speed respectively.



(a) Pattern 1



(b) Pattern 2



(c) Pattern 3

Figure 6. Water contact angles of laser-textured glass surface corresponding to laser parameters, (a) Pattern 1, (b) Pattern 2, (c) Pattern 3

For pattern 2 in Figure 6(b), the WCA range is between 43.65° and 116.12°. the WCA increases significantly with the laser power at 600 mm/min scanning speed. At 210 mm/min and 420 mm/min scanning speeds, the WCA range is 43.65°-101.24°. Samples with a lower WCA of less than 90° indicate that the laser-textured surface is in a hydrophilic state. Sample 9 recorded the highest WCA at 116.12° with 600 mm/s and 1.05 W.

In Figure 6(c), the WCA for pattern 3 ranges between 65.87° and 101.18°. The laser-textured glass surface with pattern 3 shows an increasing WCA trend as the laser power increases when processed at 210 mm/min. Sample 3 records the highest WCA of 101.18° at the highest laser power of 1.05 W. At 600 mm/s all samples are in a hydrophilic state as the WCA < 90°.

3.2 Surface Morphology

The surface morphology of laser-textured glass indicates the propagation of cracks due to laser parameters. Generally, the higher laser power and low scanning speed produced maximum crack length, while at the lower power and higher scanning speed exposure, the crack length range on the glass surface is minimal. Figure 7 shows the textured glass surfaces at different laser powers at 0.45, 0.75, and 1.05W with scanning speeds of 210, 420, and 600 mm/min. The micrographs were captured at 20× magnification to identify the effects of laser parameters on the glass surface, as shown by pattern 1, pattern 2, and pattern 3 morphology in Figures 7(a) to 7(c), respectively. The crack formation was observed on the glass surface; as the laser power increases, the finer crack lines propagate, and the glass is susceptible to cracking. In pattern 1, a narrow crack length range of 170.29-194.40 μm was measured at 0.45 W laser power; while for pattern 2, the crack length ranges between 160.0 and 246.25 μm. A wide range was measured in pattern 3 samples, where the crack length is from 143.89 to 262.03 μm. The maximum crack length range at the highest laser power varied in each pattern. Pattern 1 produced a maximum crack length range of 213.4-272.0 μm. In patterns 2 and 3, the respective range is 172.5-306.3 μm and 227.5-268.03 μm. The results suggest that the cracks spread and increase in length to reduce the surface's overall energy. Similar to previous studies shows that the crack formation was due to thermal stress during laser-surface interaction. Higher power leads to thermal shock while lower speed enhances the crack propagation due to compressive stress developed on the glass surface and tensile stress at the subsurface [34], [35].

The laser texturing produced grooves with varied widths; The heat-affected zone (HAZ) width is quite limited at low laser power, as Figure 7(a) illustrates. However, as laser power increases, so do the HAZ breadth and fracture propagation. All of the glass sample cracks have a seagull form, and one end of the crack propagates across the scanning direction; samples 5 and 6 show a significant increase in cracks, but the cracks are connected like a chain. The long crack of a line shape finally forms along the path of scanning at 0.75W, 1.05W, and 420 mm/min. Through laser processing, the morphology of the glass surface is transformed into a groove shape as the scanning speed increases and the laser intensity decreases. It is discovered that using a relatively modest scanning speed results in the groove having a very smooth surface. The groove created has a highly rough morphology as the scanning speed is increased further, however, this process condition does not nearly cause cracks around the groove [36]. Sample 4 shows burning at the groove and micron-size bubbles are seen in sample 3. The burning reaction starts at the ignition temperature on the top, at the lowest temperature at which an explosive atmosphere can ignite; thermal energy within the glass may cause thermal dissociation and other chemical reactions involving the elements listed in Table 1 when the laser beam interacts with it. This could produce oxygen gas, which could be the cause of the bubbles in the glass [36].

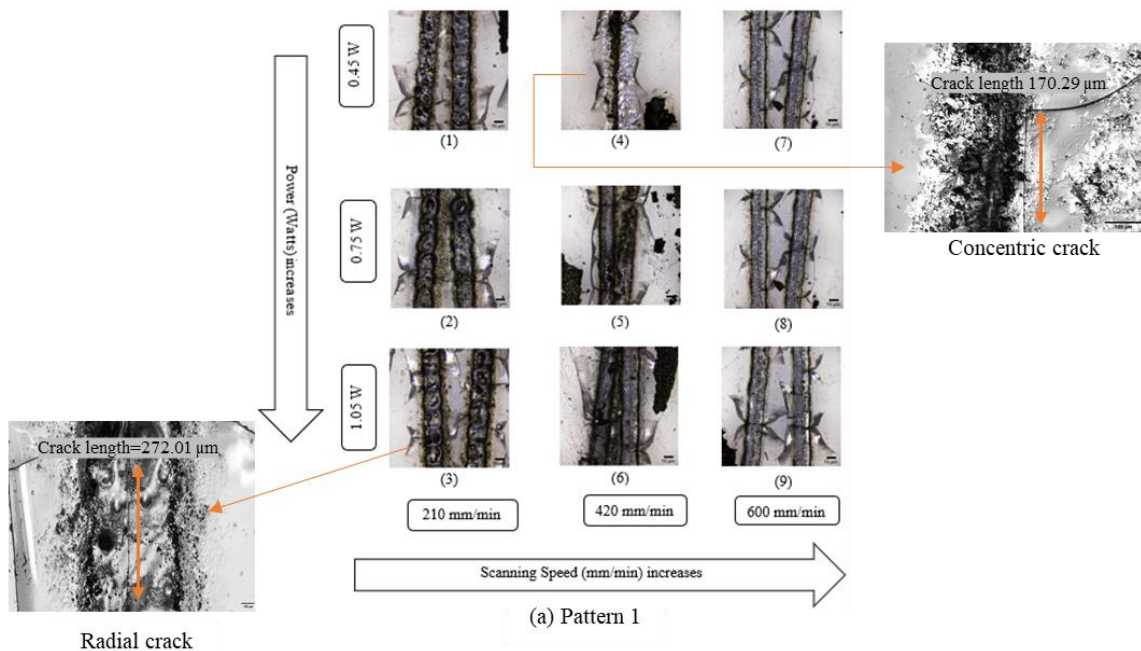


Figure 7. Surface morphology of laser textured glass surface at different laser parameters with various crack density occurrence

Figure 7(b) shows that the width of the HAZ at low power and speed has a high width compared to high power and scanning speed. The degree of thermal diffusivity, which is based on a substance's thermal conductivity, density, and specific heat in addition to the quantity of heat entering the material, affects the size of a HAZ. High thermal diffusivity materials may transport heat fluctuations more quickly, which causes them to cool more quickly and reduces the HAZ width. However, materials having a lower coefficient of thermal conductivity store heat, resulting in a wider HAZ. The quantity of heat applied, the length of time exposed to heat, and the characteristics of the material itself all affect how far the HAZ is extended. A material's HAZ is increased when it is exposed to more energy for a longer length of time [36]. All of the glass surfaces are prone to cracking; samples 1, 5, and 8 exhibit this with a seagull-shaped pattern, where tiny cracks develop, while the other sample has massive growths of cracks that are connected like a chain and reach several micrometers in size. As shown in the figure, sample 3 has an occurrence of bubbles inside the glass after laser processing; The diameter of the laser beam is significantly larger than the size of the ablation craters or bubbles. According to the table, both the height and diameter of the bubbles grow as the incident laser intensity increases. However, there are minor variations in the size of the bubbles because of the soda-lime glass's surface [36].

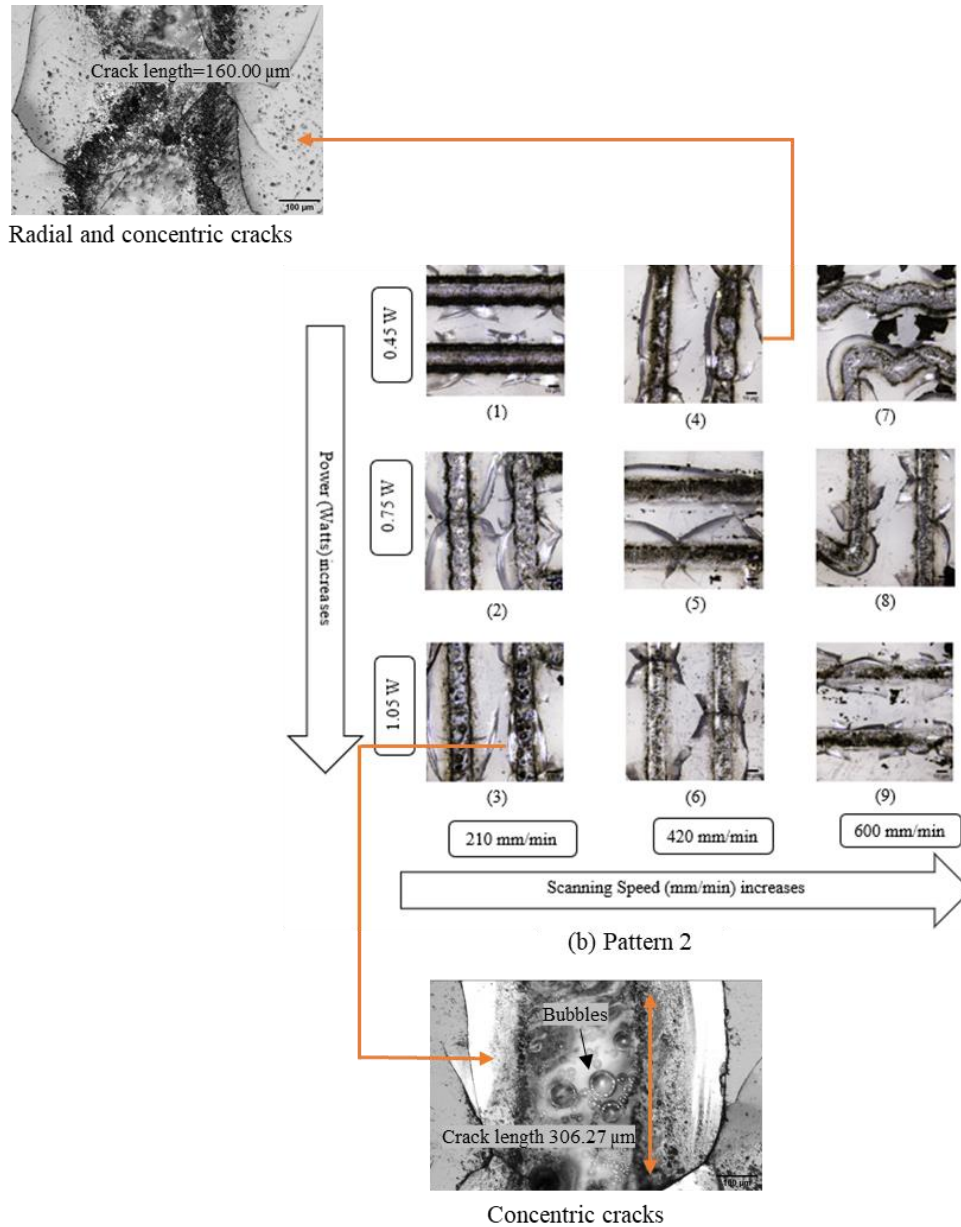


Figure 7. (cont.)

Figure 7(c), as the laser power decreases and scan speed increases, the morphology of the glass surface is turned into a groove shape through the material removal process, as shown in the figure. It is discovered that using a relatively modest scanning speed results in the groove having a very smooth surface. As demonstrated in samples 6 and 7, under these process conditions, a groove including thermal cracks is created. The groove created has a highly rough morphology as the scanning speed is increased further, however, this process condition does not nearly cause cracks to form surrounding the groove. Compared to other laser powers, low laser power had reduced HAZ. The microstructure and characteristics of this region change and become different from those of the underlying material as a result of the heating that occurs

within the HAZ. Depending on the material, these alterations may result in increased or decreased toughness, reduced corrosion resistance, higher or lower strength, or a susceptibility to cracking. These changes are typically undesired. Because of this, the HAZ is frequently a place where failures can happen [37]. Samples 6 and 7 both exhibit thermal cracks, and the crack propagation for this pattern exhibits a similar seagull-shaped crack form for all samples.

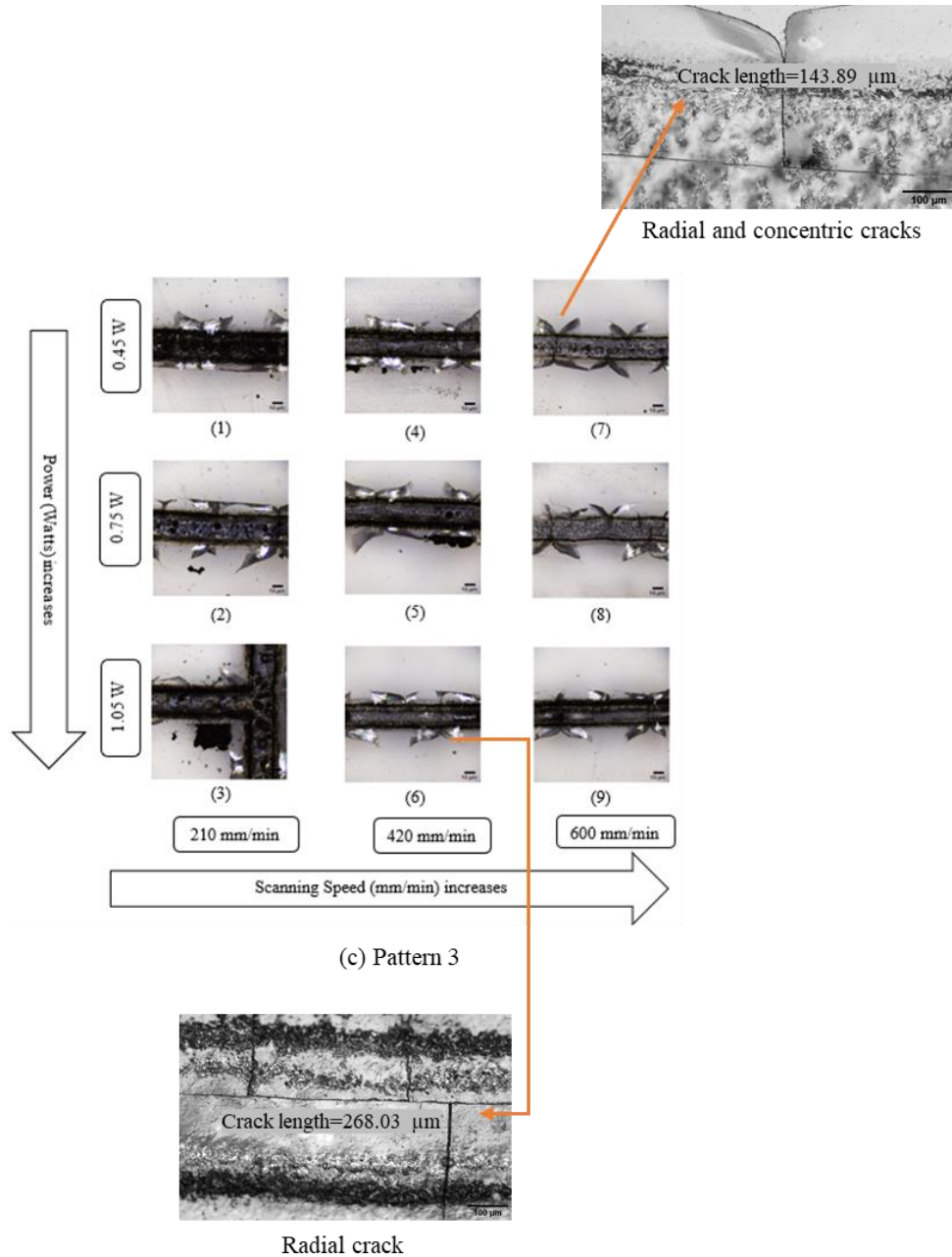


Figure 7. (cont.)

3.3 Surface Roughness

The laser-textured glass surface is characterized by its average surface roughness, Ra. The range of profile parameters obtained and the average value calculated are plotted on the graph of Figure 8. Surface roughness average, Ra measures the average length between the peaks and valleys and the deviation from the mean line on the entire surface within the sampling length. Rax represents the surface roughness average value parallel to the laser line direction, while Ray is the value of the surface roughness average perpendicular to the laser line direction.

The R² range for pattern 1 was 0.2433 and 0.2475 representing only 24% of the relationship, and the range for pattern 2 was 0.0861 and 0.2513; from these values, the surface roughness is insignificant to WCA. The range for pattern 3 was 0.5685 and 0.6171; this represents that around 50 to 60% of the roughness slightly influences the WCA. Therefore, the value of roughness observed in this experiment was inconsistent and did not affect the WCA because a surface that is too rough can result in increased friction and premature failure of a part. The results show that surface roughness can be related to the achieved wettability. The roughness of the specimen's surface improved its wettability. The hydrophilic surface grows more hydrophilic as surface roughness increases, whereas the hydrophobic section becomes more

hydrophobic as surface roughness increases [38]. This suggests the laser-textured glass surface is in a Wenzel state as the droplets spread out within the rough surface. A study by Indira et al. also presented the same trend, where higher roughness of the surface reduces the value of the WCA on the modified surface [39]. The trend of the WCA shows decrement indicating that the adhesion work increases causing the WCA to become smaller. Increasing surface roughness allows a larger solid-liquid interface which enhances the spreading work on the modified surface [40]. As scanning speed increases, surface roughness diminishes, reaching maximum Ra values below 6 μm. At low scanning speeds, the discrepancies were more noticeable, while at high scanning speeds, the roughness stabilized at minimal levels.

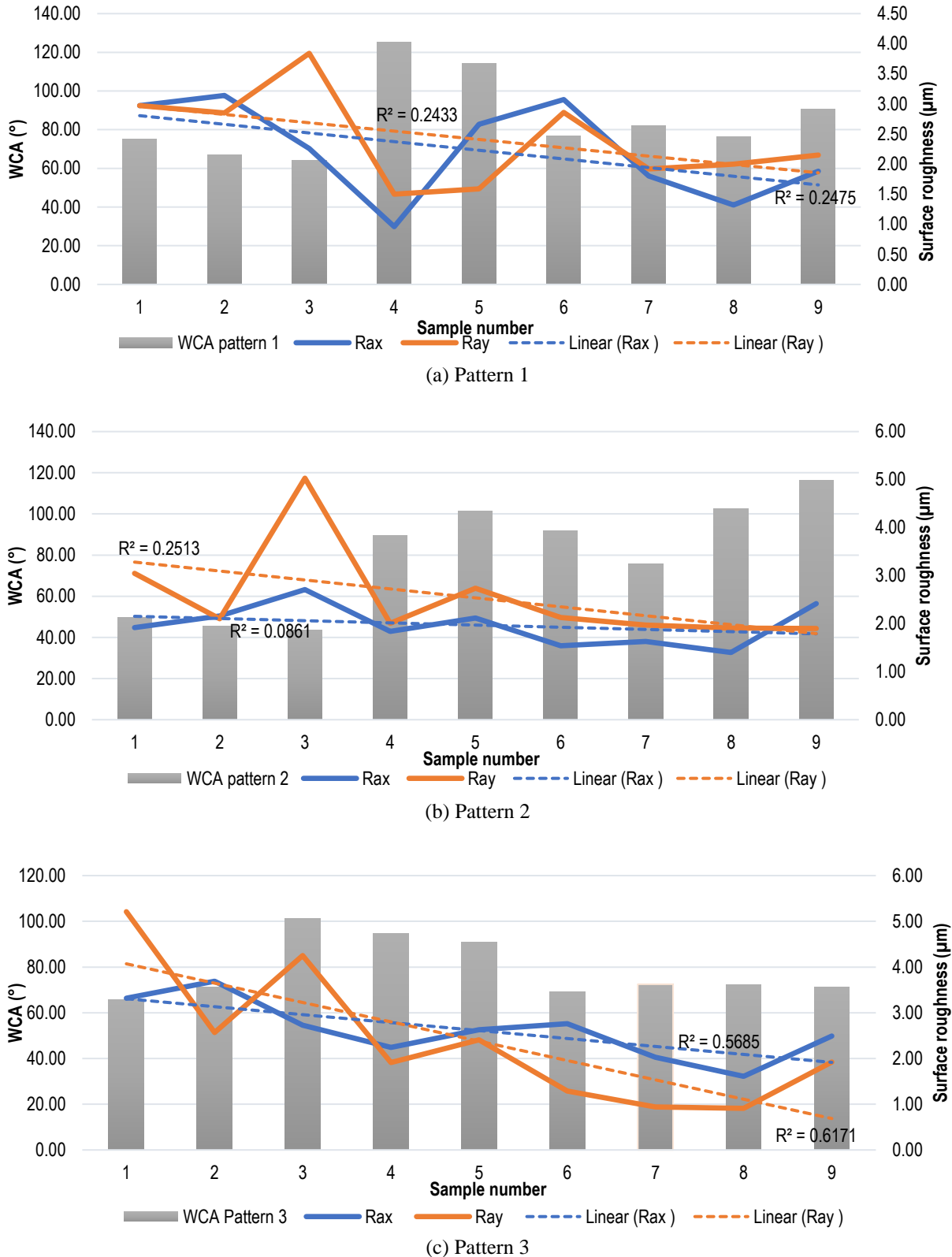


Figure 8. Graph of WCA with surface roughness, (a) Pattern 1, (b) Pattern 2, (c) Pattern 3

Figure 8(a) shows the plotted graph of WCA, and surface roughness in parallel and perpendicular to the laser line direction against the laser parameter. The highest WCA is in sample 4 at a scanning speed of 420 mm/min and laser power at 0.45 W has the lowest value of surface roughness R_{ax} and R_{ay} at 0.96 and 1.5 μm . The lowest WCA at a scanning speed of 210 mm/min and the highest laser power at 1.05 W show a vast gap between R_{ax} and R_{ay} values. R_{ay} for sample 3 had the highest value at 3.84 μm while for R_{ax} at 2.26 μm . The smallest difference between the surface profile value of parallel and perpendicular direction produces a higher WCA.

Figure 8(b) shows the relationship between WCA and roughness profile for pattern 2. At the lower scanning speed of 210 mm/min, the values of R_{ax} and R_{ay} are higher than 420 and 600 mm/min. Sample 3 recorded the highest value of R_{ax} and R_{ay} at 2.72 and 5.03 μm and the lowest WCA at 43.65°. For samples 5, 8, and 9 (sample processing conditions at higher laser power and scanning speed), higher WCAs of 101.24°, 102.45°, and 116.12° were achieved, but lower values of R_{ax} and R_{ay} compared to sample 3. The trend of R_a shows decreasing profile roughness as it approaches the higher scanning speed and produces higher WCA.

The relationship between WCA and roughness profile for pattern 3 in Figure 8(c) shows sample 1 with the highest value of R_{ay} at 5.21 μm and the lowest WCA at 63.87°. Sample 3 processed at a lower scanning speed and a high laser power, has a slight decrease in R_{ay} at 4.25 μm and the highest WCA at 101.18°. The trend of R_a values shows an irregular pattern with no correlation with the water contact angle measured. Therefore, the profile does not influence the WCA measurement on the modified surface.

4.0 CONCLUSIONS

This experimental work and study investigated the effect of laser processing parameters on the surface wettability of soda lime glass. According to our findings, the surface can change from hydrophilic to hydrophobic with a contact angle of up to 125.29°. The highest WCA was measured on the glass surface that was textured with pattern 1 consisting of a range of line distances between 0.14 and 1.00 mm. The respective line distance in patterns 2 and 3 was 0.5 and 1.0 mm. These patterns produced the highest WCA of 116.12° and 101.18°, which is contributed by the line distance difference. Patterns 1 and 2 produced a similar trend with increasing WCA at the highest scanning speed. During surface modification, the effects of laser power and scan speed were examined. Upon observing the micrographs of the modified glass surface, defects like bubbles and radial and concentric line cracks were observed on the laser-textured glass surface. In addition, the crack length increases as the laser power increases. Also, the irregular surface profile of laser-textured glass indicates the samples are in a Wenzel state, where higher surface roughness enhanced wettability that reduced the WCA. To design possible engineering applications, like self-cleaning glass, this paper offers parameter recommendations and a solid foundation for modifying the hydrophobicity of soda-lime glass surfaces with the use of laser texture parameters. Therefore, choosing appropriate and optimal laser processing parameters is essential to determine whether the result will be an improvement in surface wettability or the opposite. Future research will need to examine additional variables that affect surface wettability, such as chemical composition and surface energy. However, surface wettability can be transformed and changed by utilizing laser processing methodology to regulate the surface texture.

5.0 ACKNOWLEDGEMENT

The authors would like to acknowledge the financial support from the Ministry of Higher Education Malaysia under Fundamental Research Grant Scheme FRGS/1/2021/TK0/UMP/02/48 (UMP grant no: RDU210145) for funding this research.

6.0 REFERENCES

- [1] K. Ellinas, P. Dimitrakellis, P. Sarkiris, and E. Gogolides, "A review of fabrication methods, properties and applications of superhydrophobic metals," *Processes*, vol. 9, no. 4, p. 666, 2021.
- [2] K. Manoharan and S. Bhattacharya, "Superhydrophobic surfaces review: Functional application, fabrication techniques and limitations," *Journal of Micromanufacturing*, vol. 2, no. 1, pp. 59-78, 2019.
- [3] S. A. Getaneh, A. G. Temam, A. C. Nwanya, P. M. Ejikeme, and F. I. Ezema, "Advances in bioinspired superhydrophobic surface materials: A review on preparation, characterization and applications," *Hybrid Advances*, vol. 3, p. 100077, 2023.
- [4] S. Parvate, P. Dixit, and S. Chattopadhyay, "Superhydrophobic Surfaces: Insights from Theory and Experiment," *Journal of Physical Chemistry B*, vol. 124, no. 8, pp. 1323–1360, 2020.
- [5] P. Liu, X. Bai, W. Xing *et al.*, "Translucent and superhydrophobic glass for self-cleaning and acid rain-restraining," *Materials Chemistry and Physics*, vol. 259, no. September 2020, p. 124049, 2021.
- [6] J. E. Adukwu, B. S. Yilbas, A. S. Jalilov *et al.*, "Adhesion characteristics of solution treated environmental dust," *Scientific Reports*, vol. 10, no. 1, pp. 1–15, 2020.
- [7] S. Maharjan, K-S. Liao, A. J. Wang *et al.*, "Self-cleaning hydrophobic nanocoating on glass: A scalable manufacturing process," *Materials Chemistry and Physics*, vol. 239, no. July 2019, p. 122000, 2020.
- [8] M. Vasiliev, V. Rosenberg, J. Lyford, and D. Goodfield, "Field Performance Monitoring of Energy-Generating High-Transparency Agrivoltaic Glass Windows," *Technologies*, vol. 11, no. 4, 2023.

- [9] O. Rius-ayra and N. Llorca-isern, "Special issue 'surface modification of metals and alloys,'" *Coatings*, vol. 11, no. 2, pp. 1–3, 2021.
- [10] N. P. Prorokova, O. I. Odintsova, V. E. Rummyantseva, E. V. Rummyantsev, and V. S. Konovalova, "Giving Improved and New Properties to Fibrous Materials by Surface Modification," *Coatings*, vol. 13, no. 1, pp. 1–22, 2023.
- [11] A. F. Gouveia, L. Gracia, E. Longo, M. A. San-Miguel, and J. Andrés, "Modulating the properties of multifunctional semiconductors by means of morphology: Theory meets experiments," *Computational Materials Science*, vol. 188, p. 110217, 2021.
- [12] M. Mozetič, "Surface modification to improve properties of materials," *Materials (Basel)*, vol. 12, no. 3, p. 441, 2019.
- [13] A. Rosenkranz, H. L. Costa, M. Z. Baykara, and A. Martini, "Synergetic effects of surface texturing and solid lubricants to tailor friction and wear – A review," *Tribology International*, vol. 155, no. October 2020, p. 106792, 2021.
- [14] S. K. Nemani, R. K. Annavarapu, B. Mohammadian *et al.*, "Surface modification of polymers: Methods and Applications," *Advanced Materials Interfaces*, vol. 5, no. 24, p. 1801247, 2018.
- [15] K. Ellinas, *Superhydrophobic and superamphiphobic smart surfaces*, Elsevier, pp. 487-514, 2019.
- [16] Z. Wang, J. Kong, Q. Zhou, and X. Chen, "Natural Superhydrophobic Surfaces and Application," *Journal of Physics: Conference Series*, vol. 2390, no. 1, p. 012115, 2022.
- [17] D. Wang, Q. Sun, M. J. Hokkanen *et al.*, "Design of robust superhydrophobic surfaces," *Nature*, vol. 582, no. 7810, pp. 55–59, 2020.
- [18] Z. Wang, S. Paul, L. H. Stein, A. Salemi, and S. Mitra, "Recent Developments in Blood-Compatible Superhydrophobic Surfaces," *Polymers (Basel)*, vol. 14, no. 6, p. 1075, 2022.
- [19] K. Manoharan and S. Bhattacharya, "Superhydrophobic surfaces review: Functional application, fabrication techniques and limitations," *Journal of Micromanufacturing*, vol. 2, no. 1, pp. 59–78, 2019.
- [20] B. W. Chieng, N. A. Ibrahim, N. A. Daud, and Z. A. Talib, "Functionalization of graphene oxide via gamma-ray irradiation for hydrophobic materials," In *Synthesis, technology and applications of carbon nanomaterials*, Elsevier, pp. 177-203, 2018.
- [21] M. Sun, N. Kumar, A. Dhinojwala, and H. King, "Adhesive forces inhibit underwater contact formation for a soft-hard collision," 2021, [Online]. Available: <http://arxiv.org/abs/2102.10789>.
- [22] Y. Sun, Y. Li, X. Dong, X. Bu, and J. W. Drelich, "Spreading and adhesion forces for water droplets on methylated glass surfaces," *Colloids and Surfaces A: Physicochemical and Engineering*, vol. 591, p. 124562, 2020.
- [23] A. Ouchene, G. Mollon, M. Ollivier *et al.*, "Roughness and wettability control of soda-lime silica glass surfaces by femtosecond laser texturing and curing environments," *Applied Surface Science*, vol. 630, no. April, p. 157490, 2023.
- [24] S. Xiao, X. Hao, Y. Yang, L. Li, N. He, and H. Li, "Feasible fabrication of a wear-resistant hydrophobic surface," *Applied Surface Science*, vol. 463, no. May 2018, pp. 923–930, 2019.
- [25] T. Liu, Y. Yin, S. Chen, X. Chang, and S. Cheng, "Super-hydrophobic surfaces improve corrosion resistance of copper in seawater," *Electrochimica Acta*, vol. 52, no. 11, pp. 3709–3713, 2007.
- [26] S. Basset, G. Heisbourg, A. Pascale-Hamri, S. Benayoun, and S. Valette, "Effect of texturing environment on wetting of biomimetic superhydrophobic surfaces designed by femtosecond laser texturing," *Nanomaterials*, vol. 12, no. 18, p. 3099, 2022.
- [27] B. Wang, Y. Hua, Y. Ye, R. Chen, and Z. Li, "Transparent superhydrophobic solar glass prepared by fabricating groove-shaped arrays on the surface," *Applied Surface Science*, vol. 426, pp. 957–964, 2017.
- [28] K. Liao, W. Wang, X. Mei *et al.*, "Stable and drag-reducing superhydrophobic silica glass microchannel prepared by femtosecond laser processing: Design, fabrication, and properties," *Materials and Design*, vol. 225, p. 111501, 2023.
- [29] R. Coatings, "Standard Practice for Surface Wettability of Coatings, Substrates and Pigments by Advancing Contact Angle Measurement," *Annual Book ASTM Standards*, vol. I, no. C, 2011.
- [30] ASTM D7490, "ASTM D7490: Measurement of the Surface Tension of Solid Coatings, Substrates and Pigments using Contact Angle Measurements", 2013.
- [31] H. H. Nguyen, A. K. Tieu, S. Wan, H. Zhu, S. T. Pham, and B. Johnston, "Surface characteristics and wettability of superhydrophobic silanized inorganic glass coating surfaces textured with a picosecond laser," *Applied Surface Science*, vol. 537, p. 147808, 2021.
- [32] K. Indira, C. Sylvie, W. Zhongke, and Z. Hongyu, "Investigation of wettability properties of laser surface modified rare earth Mg alloy," *Procedia Engineering*, vol. 141, pp. 63–69, 2016.
- [33] X. Jing, Y. Xia, F. Chen, C. Yang, Z. Yang, and S. H. I. Jaffery, "Preparation of superhydrophobic glass surface with high adhesion," *Colloids and Surfaces A: Physicochemical and Engineering Aspects*, vol. 633, p. 127861, 2022.
- [34] D.-L. Kim and B.-T. Kim, "Crack formation process in ceramic Nd:YAG," *OSA Continuum*, vol. 3, no. 6, p. 1633, 2020.
- [35] J. Y. Kim, K. Cho, S. Ryu, S. Y. Kim, and B. M. Weon, "Crack formation and prevention in colloidal drops," *Science Report*, vol. 5, no. 1, p. 13166, 2015.
- [36] J. Shin and K. Nam, "Groove formation in glass substrate by a UV nanosecond laser," *Applied Sciences*, vol. 10, no. 3, pp. 6–7, 2020.
- [37] T. Haz and T. Haz, "What is the heat affected zone (HAZ)?," pp. 1–9, 2023, [Online]. Available: What is the Heat Affected Zone (HAZ)? - TWI (twi-global.com).

- [38] F. P. Prakash, N. Jeyaprakash, M. Duraiselvam, G. Prabu, and C. H. Yang, "Droplet spreading and wettability of laser textured C-263 based nickel superalloy," *Surface and Coatings Technology*, vol. 397, p. 126055, 2020.
- [39] Y. Guan, S. Zhang, J. Li, X. Tian, and H. Zheng, "Laser surface processing of magnesium alloys," In *Machining of Light Alloys*, CRC Press, pp. 125–150, 2018.
- [40] J. Wang, Y. Wu, Y. Cao, G. Li, and Y. Liao, "Influence of surface roughness on contact angle hysteresis and spreading work," *Colloid and Polymer Science*, vol. 298, no. 8, pp. 1107–1112, 2020.